IOP Conf. Series: Materials Science and Engineering **278** (2017) 012090 doi:10.1088/1757-899X/278/1/012090

Impact of large beam-induced heat loads on the transient operation of the beam screens and the cryogenic plants of the Future Circular Collider (FCC)

H Correia Rodrigues[1], **L Tavian**[1]

[1]CERN, CH-1211 Geneva 23, Switzerland

E-mail: laurent.tavian@cern.ch

Abstract. The Future Circular Collider (FCC) under study at CERN will produce 50-TeV high-energy proton beams. The high-energy particle beams are bent by 16-T superconducting dipole magnets operating at 1.9 K and distributed over a circumference of 80 km. The circulating beams induce 5 MW of dynamic heat loads by several processes such as synchrotron radiation, resistive dissipation of beam image currents and electron clouds. These beam-induced heat loads will be intercepted by beam screens operating between 40 and 60 K and induce transients during beam injection. Energy ramp-up and beam dumping on the distributed beam-screen cooling loops, the sector cryogenic plants and the dedicated circulators. Based on the current baseline parameters, numerical simulations of the fluid flow in the cryogenic distribution system during a beam operation cycle were performed. The effects of the thermal inertia of the headers on the helium flow temperature at the cryogenic plant inlet as well as the temperature gradient experienced by the beam screen has been assessed. Additionally, this work enabled a thorough exergetic analysis of different cryogenic plant configurations and laid the building-block for establishing design specification of cold and warm circulators.

1. Introduction

The Future Circular Collider (FCC) will use electric fields to speed up and increase the energy of a beam of particles [1,2]. During this process, a variable amount of synchrotron radiation emission from the charged particles takes place. To prevent this power from impinging on the superconducting magnets, a beam screen is used. This, in turn, requires that several parameters in the cryogenic plants are adjusted to accommodate the variations of refrigeration power needed to control the temperature of the beam-screen and, ultimately, ensure a good vacuum quality. The time constants of these parameters are not necessarily compatible with the dynamic heat loads resulting from the increase in energy of the circulating beams, making the cryogenic plants design a top priority issue.

This study focuses on the assessment of: (1) the performance of the cryogenic plants and (2) the ability of the compressors to accommodate transient operational regimes resulting from the beam-induced heat loads. The results were based on two-beam cycles and the analysis performed for the arc sector of the FCC (see Figures 1 and 2).

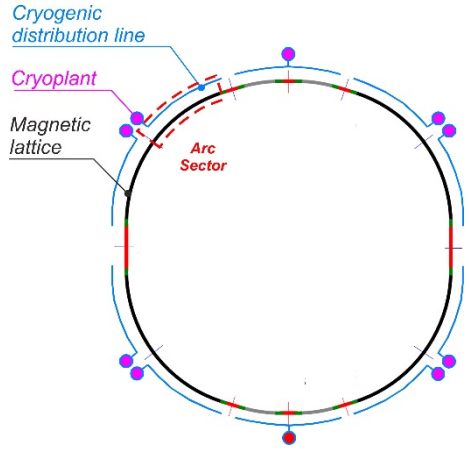

Figure 1. FCC layout.

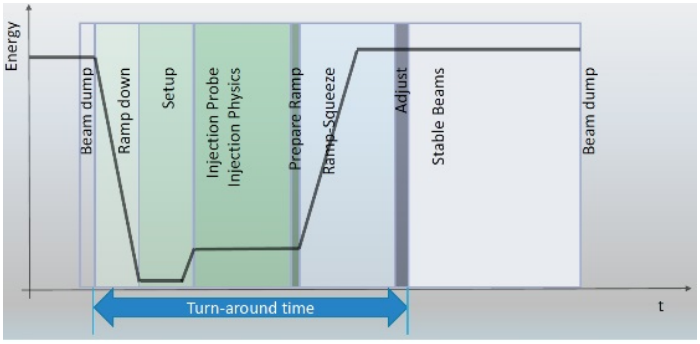

Figure 2. Schematic of the FCC beam cycle.

2. Arc sector baseline parameters

The FCC is foreseen to have two sections for high-luminosity experiments and two others for low-luminosity experiments. Therefore, two beam cycles were considered in this study: the high-luminosity beam, with a total beam cycle of about 9 hours and low-luminosity, with a total beam cycle of about 16 hours.

The length of the arc sector is of 8493 m (see Figure 1). It is comprised of 79 half-cells. Each individual half-cell measures 107.1 m and consists of an array of 7 magnets, one quadrupole and six dipoles.

The FCC will have a beam-screen inserted in the vacuum pipes to intercept the heat loads resulting from the circulating particle beams (see Figure 3). A flow of helium circulates in cooling channels of the beam screen to ensure its operation between 40 and 60 K. The beam screen is designed to withstand a maximum pressure of 50 bar [3,4].

3. Cryogenic distribution layout and heat loads

The helium flow is cooled by a turbo-Brayton cycle using a mixture of neon-helium as working fluid [5]. Throughout a beam cycle, the helium flow in the supply header is maintained at a constant temperature of 40 K (see Figure 3). The beam screen circuit is fed with cooling fluid every half-cell. The helium exiting the beam-screen is then used to cool the thermal shield and, ultimately, flows across the return header to the cryogenic plant. The thermal shield is made of aluminium and has a specific weight of about 32 kg/m. The return header is comprised of stainless steel and aluminium and has specific weight of 40 kg/m.

For the FCC, every beam cycle is a sequence made of tightly coupled tasks that need to be carried out in strict order to make a transition from one state to another. In broad terms, the beam cycle is comprised of four main steps: setup, ramping, stable beams and beam dump. During the setup phase, all the accelerators systems are tested and prepared for the injection of the particle beams. This, in turn, results in a linearly increase of image current. At the end of the setup stage, the heat load intercepted by the beam-screen is 3 W/m. The setup stage is preceded by the injection of batches from the LHC and the ramping of the superconducting magnets. For every passage across the radio-frequency cavities, the energy of the circulating beams is increased. Consequently, the synchrotron radiation emitted by the charged particles being radially accelerated increases dramatically. Once the desired energy of the circulating beams is achieved, a stage of stable beams is entered. The heat load intercepted by the beam screen due to synchrotron radiation and image current is of 30 W/m per beam, i.e. 60 W/m. The particle beams collide for several hours and are eventually dumped.

To ensure the beam screen temperature does not exceed 60 K at any given location in the arc, an identical mass flow rate of 71 g/s is fed into each individual half-cell. The flow exiting each half-cell

mixes with the incoming flow in the return header. Thus, as a result of the cryogenic distribution line architecture, the mass flow rate in the return header at the end of the arc is substantially smaller than those near the cryogenic plant. An important implication is that the flow velocities at the end of the sector are about 2 orders of magnitude smaller than those encountered at the beginning.

During a given beam cycle, the cryogenic distribution system is foreseen to operate between 40 to 60 K. Considering a beam cycle wherein the compressors operate at a constant discharge pressure results in variations of the mass of helium in the cryogenic distribution system of about 6 tons per cycle. This implies the mass would have to be transported back and forth to the cryogenic plants per each beam cycle. To counteract this effect, the discharge pressure of the compressor units is deliberately changed throughout the beam cycle to compensate for any variation of mass of helium by the beam-induced heat loads.

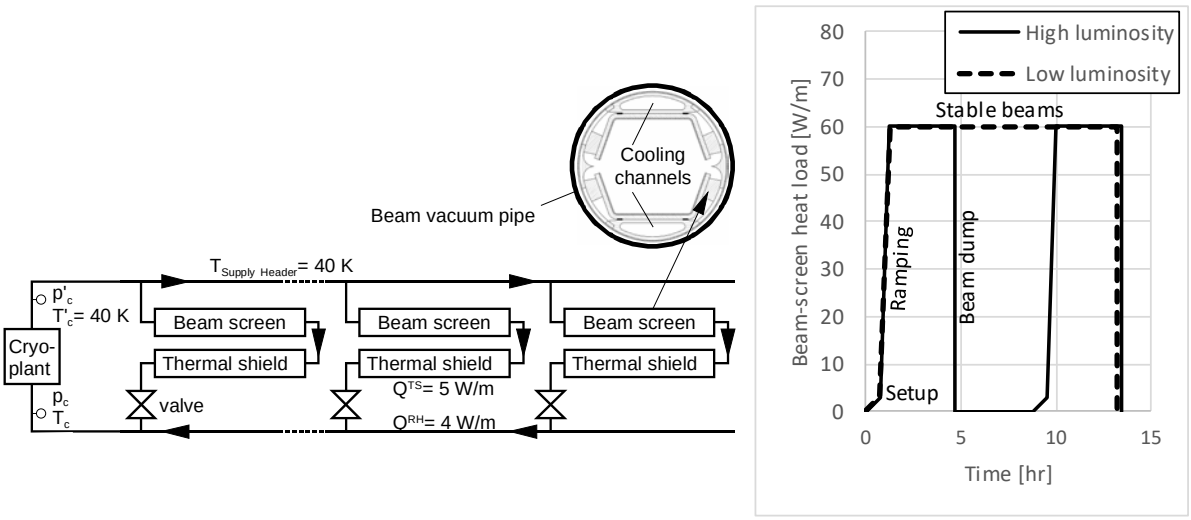

Figure 3. Schematic of the cryogenic distribution line showing static and dynamic heat-loads (the static heat-loads in the supply header are considered negligible).

4. Mathematical modelling of the cryogenic distribution line

A model based on 1-dimensional Navier-Stokes and energy equations was derived to study the cryogenic distribution system behaviour over a beam cycle. Under the assumption that the temperature gradients in the radial and longitudinal directions are small, the aforementioned equations can be reduced to a set of 1-dimensional partial differential equations. The dynamic and static heat loads are represented in the partial equations by source terms. Then, the differential equations are then discretized by Euler methods and implemented in *Spyder*, an open source platform for scientific programming in *Python* language.

5. Cryogenic plants configuration

To evaluate the operational costs of the different types of compressors, two cryogenic plant architectures were considered in this study (see Figure 4): (1) cold scheme, featuring a compressor operating in the desired temperature range of the beam-screen and (2) warm scheme, featuring a compressor operating at ambient temperature.

The isentropic efficiency of the cold and the warm compressor was assumed to be 70% and 86%, respectively. In the following analysis, the pressure drop across the different elements of the cryogenic plants are considered negligible with respect to the pressure drop developed in the cryogenic distribution. The NTU of the heat exchanger was assumed to be 40. As a result, the temperature difference between the two streams at one end of the heat exchanger is of 5 K.

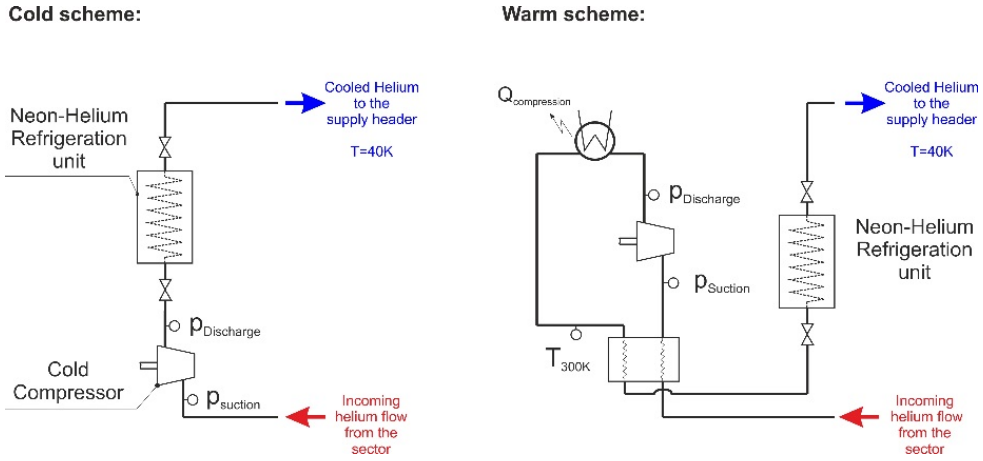

Figure 4. Schematic of the cold and warm compressor installed in the cryogenic plants.

6. Results

6.1 High-luminosity beam cycle

6.1.1. Dynamics of the helium pressure and temperature due to beam-induced heat loads. Figure 5 shows the evolution of the beam-induced heat loads, the pressure and the temperature over a high-luminosity beam cycle. The pressure and temperature at the beginning of the supply header are shown by a solid line (p'_c and T'_c, respectively). The corresponding pressure and temperature in the return header is shown by a dashed line (p_c and T_c, respectively). Hereinafter, the prime symbol refers to the physical properties of the helium flow at the beginning of the sector (see Figure 3). Figure 6 shows the temperature evolution of the helium flow and of the thermal shield after dumping the particle beams. In Figure 7, the temperature profiles of the helium flow across the return header over a high-luminosity beam cycle are plotted. Figures 5, 6 and 7 are used for the following analysis. The figures are presented to support the authors' interpretations and serve as an additional verification for the soundness of the hypothesis presented herein.

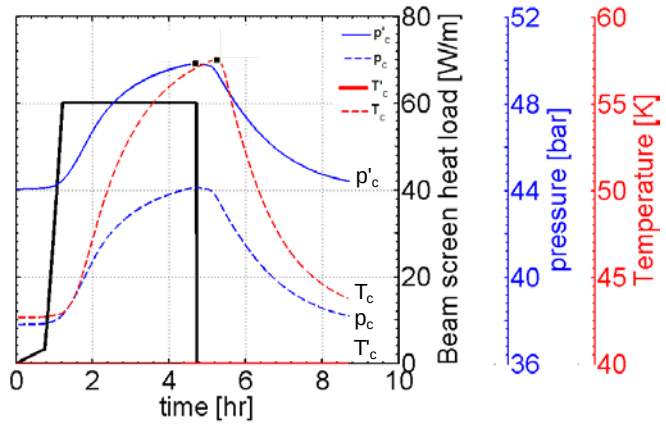

Figure 5. Beam screen heat load, pressure and temperature evolution over a high-luminosity beam cycle.

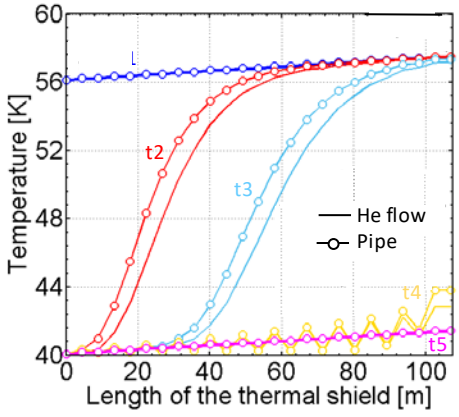

Figure 6. Helium and pipe temperature distribution across the thermal shield after the beam dump (t1= 4.7 hr, t2= 4.8 hr, t3= 5.0 hr, t4= 5.3 hr and t5= 8.7 hr).

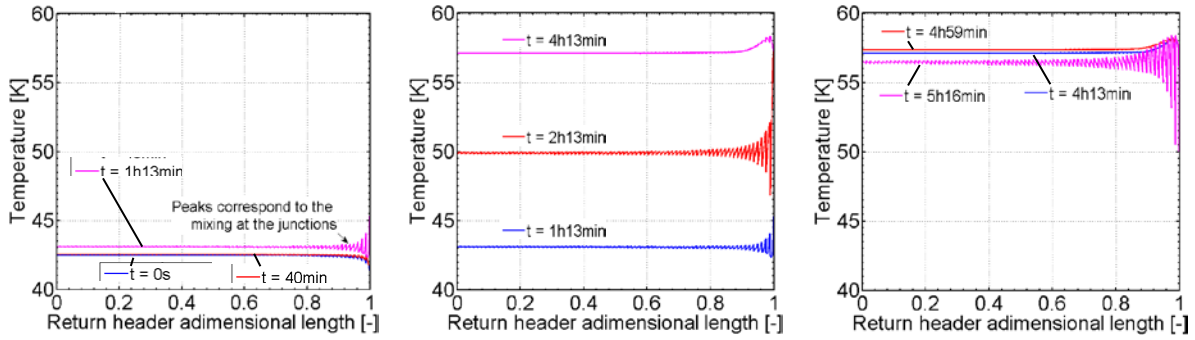

(a) Setup and ramping (b) Stable beams (c) Beam dump

Figure 7. Temperature profiles across the return header over a high-luminosity beam cycle. The length of the total return header is of 8493 m.

The results of Figure 5 show that the behaviour of the pressure is qualitatively different from that of the temperature. During the setup stage, the heat load due to the image current increases linearly to 3 W/m. No substantial changes of T_c are observed, however, a mild increase of p'_c is witnessed. This occurs as a result of the increase of the helium temperature. The gradual variations in the temperature result in changes of the mass of helium contained in the beam screen and the return header through the effects of the density. To counteract the influence of the temperature and thus maintain a constant mass of helium in the cryogenic distribution system, p'_c increases. This, in turn, implies that the operational parameters of the compressor units (e.g. rotating speed) change to augment the discharge pressure.

The setup stage is followed by the injection of the particle beams and the ramping of the magnets. The heat load intercepted by the beam screen is substantially increased due to the synchrotron radiation emitted by the circulating beams (see Figure 5). Accordingly, p'_c and T_c increase with a more pronounced increase for p'_c.

Once the desired energy of the particle beams is reached, collisions are initiated in the detectors. Whilst the experimental campaigns take place, synchrotron radiation remains constant, and p'_c and T_c continue to increase.

At the end of the experimental campaign, the particle beams are deliberately dumped. As a result, the synchrotron radiation emanated by the circulating beams ceases to exist. Whilst no beam-induced heat loads are present, it can be observed that T_c continues to rise for about 40 mins until it eventually starts decaying. This observation is contrasted with the decrease of p'_c.

These observations stem from the decrease of the helium temperature in the beam screen, and the thermal inertia of the thermal shield and the return header. The beam screen has a low specific weight compared to other elements in the cryogenic distribution system. Then, as the beam is dumped, the beam screen quickly decreases its temperature to 40 K. As a result, the mass of helium contained in cooling channels of the beam screen increases. To maintain the total mass of helium constant in the cryogenic distribution system, this effect is compensated by a decrease of p'_c which, by implication, results in a decrease of the fluid density.

The helium flow exiting the beam screen at 40 K encounters a thermal shield at about 56 K (see Figure 6). The helium flowing in the thermal shield is heated-up and exits at 56 K for about 20 mins. Over this period, each thermal shield continuously feeds the return header with a helium flow at 56 K and, therefore, T_c continues to rise.

A further contributor to the continuous increase of T_c is the return header. As the temperature of the helium flow exiting the thermal shield drops, it encounters a return header at a higher temperature and a similar behaviour can be seen. The temperature of the helium flow exiting the return header eventually drops and T_c progressively decreases for about 4 hours. It is worth noting that during a high-luminosity beam cycle the cryogenic system does not reach a steady state.

6.1.2. Refrigeration power and exergetic efficiency. Figure 8 shows the evolution of the compressor and refrigeration power over a high-luminosity beam cycle. To evaluate the performance of the cold and the warm schemes, the exergetic efficiency as a function of time was also plotted.

The results show that the power required by the cold compressor is of about 130 kW and substantially smaller than that of the warm compressor. The transient experienced by the neon-helium refrigeration unit does not differ for the two schemes studied herein. However, the cold scheme presents an advantage with regard to exergetic efficiency. This stems from the inefficiency pertaining to the heat exchanger. It is worth noting that the exergetic efficiency per beam cycle can be considerably improved by increasing the heat exchanger NTU and, therefore, decrease the temperature of the stream exiting the heat exchanger towards the neon-helium plant.

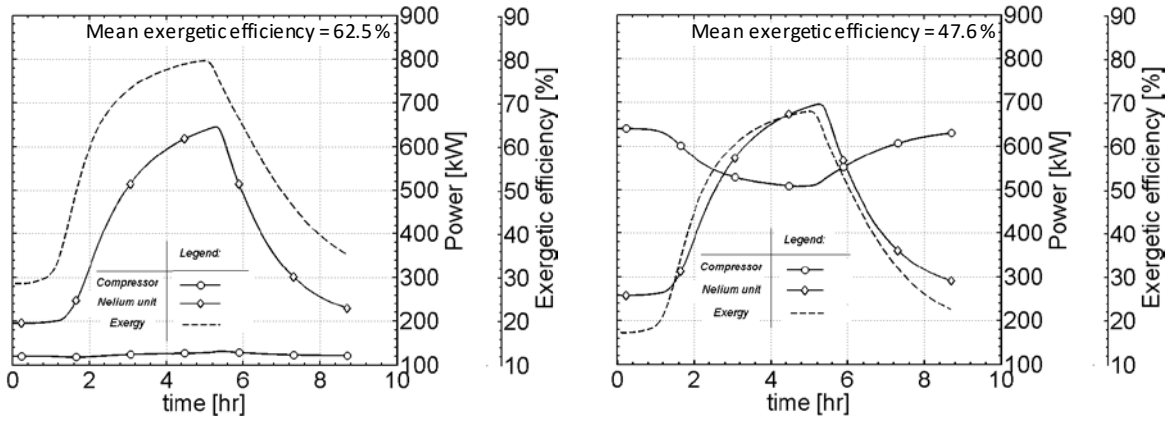

(a) Cold scheme (b) Warm scheme

Figure 8. Transient behavior of the cryoplants over a high-luminosity beam cycle.

6.2 Low-luminosity beam cycle

6.2.1 Dynamics of the helium pressure and temperature due to beam-induced heat loads. Figure 9 shows the evolution of the beam-induced heat loads, the pressure and the temperature over a low-luminosity beam cycle. The results are presented in a similar fashion as Figure 5 to bring out the most notable features of p'_c and T_c over a low-luminosity beam cycle.

The trends encountered in Figure 9 are identical to those of Figure 5 and can be explained by similar arguments: the decrease of the helium temperature in the beam screen and the thermal inertia of the thermal shield and the return header. Although the same qualitative behaviour can be found, a steady state is reached during the stable beam stage.

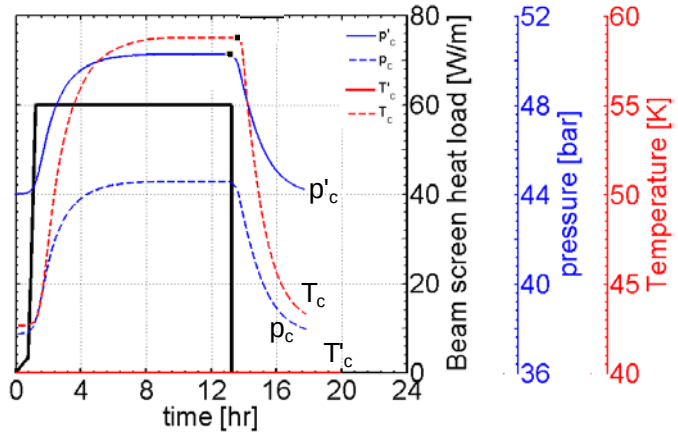

Figure 9. Beam screen heat load, pressure and temperature evolution over a low-luminosity beam cycle.

6.2.2 Refrigeration power and exergetic efficiency. Figure 10 shows the evolution of the compressor and refrigeration power over a low-luminosity beam cycle. Qualitatively, both the refrigeration power and the exergetic efficiency exhibit the same behaviour observed in Figure 8. The period of time over which the beam-induced heat loads are at its maximum value is considerably larger than that of the high-luminosity cycle. The implication is that the cryogenic plants operate over longer periods of time at higher exergetic efficiencies. As a result, the mean average exergetic efficiency per beam cycle is greatly increased.

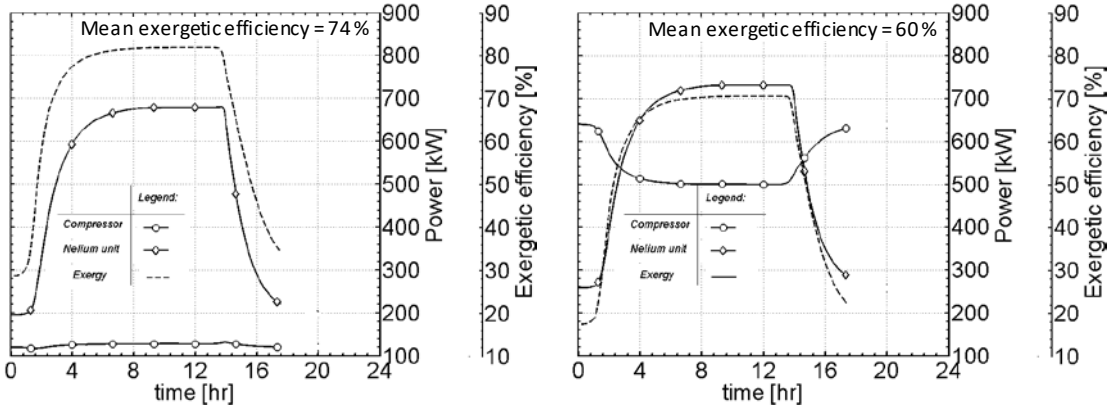

(a) Cold scheme (b) Warm scheme

Figure 10. Transient behavior of the cryoplants over a low-luminosity beam cycle.

6.3 Compression fields

The variation of pressure ratio and reduced mass flow rate over two beam cycles is plotted in Figure 11. The reduced mass flow rate for a hydrodynamic compressor is defined as:

$$\dot{m}_R = \dot{m}_{He}\sqrt{\frac{T}{T_0}}\frac{p_0}{p} \tag{1}$$

For the cold scheme, T_0 and p_0 correspond to the values of p_c and T_c in steady state conditions, i.e. 44 bar and 60 K.

The markedly different compression fields can be explained by the evolution of the pressure and temperature at the suction of the compressors. For the cold scheme, the rationale is the following. During the setup stage, no substantial changes of T_c are observed, however, a mild increase of p_c is witnessed. This effect is accompanied by a reduction of the flow velocity in the headers and, consequently, a reduction of the pressure drop across the headers. The result is a decrease of $\dot{m}_R$ through the effects of p_c. Once T_c starts increasing, a different behaviour is witnessed. Specifically, an increase of T_c, leads to a cancellation effect, and the reduced mass flow rate begins to increase. When the beam is dumped, discharge pressure of the compressor is decreased. This, in turn, contributes further to the increase of $\dot{m}_R$. When T_c starts decreasing, $\dot{m}_R$ ceases to increase and reverses its direction.

For the warm scheme, the temperature at the suction of the compressor remains constant throughout the beam cycle. Hence, $\dot{m}_R$ becomes inversely proportional to p_c and depends uniquely on the pressure at the suction of the compressor. During the setup stage and the ramping, an increase of p_c is witnessed and, therefore, $\dot{m}_R$ continuously decreases. Once the beam is dumped, p_c increases and the opposite behaviour is observed.

The reduced flow variation is less than +/-1 % for the cold compressor and +18 % for the warm compressor. These variations are fully compatible with the operating ranges of hydrodynamic machines.

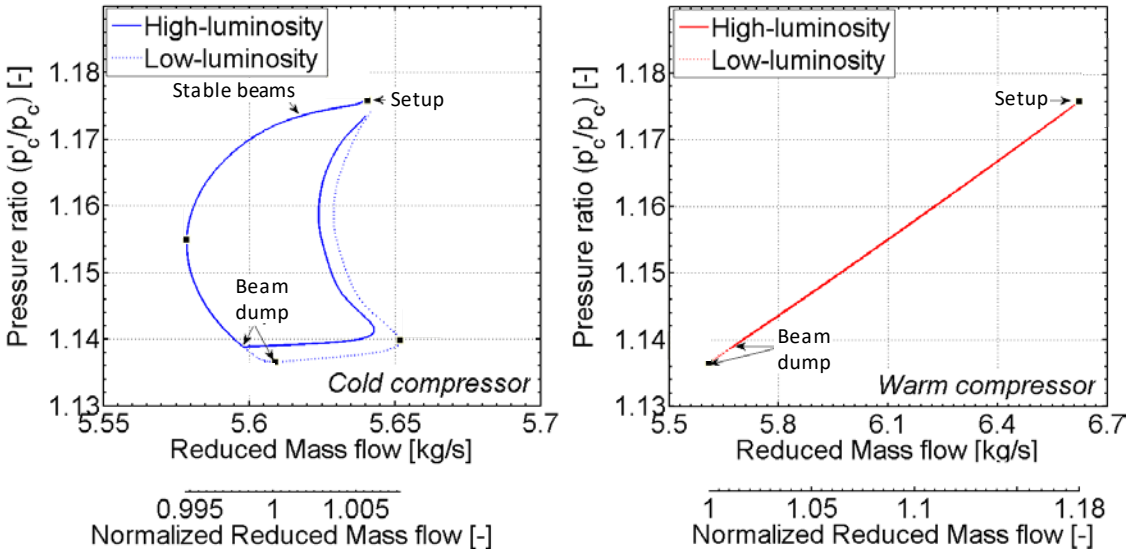

Figure 11. Compression fields for the cold and the warm scheme.

7. Conclusions

In this study, the transient behaviour of the cryogenic plants and the compressor units was evaluated for a high- and low-luminosity beam cycle. The results enabled to define the technical specifications of the compressors and the neon-helium refrigeration units as well as to identify an economically viable solution for the future cryogenic facilities.

Acknowledgments

The authors would like to thank Daniel Schulte and Cedric Garion for the beam design and beam cycle specifications.

References

[1] Lebrun Ph and Tavian L, Beyond the Large Hadron Collider: a first look at cryogenics for CERN future circular colliders, 25th ICEC Conference, Twente, Netherland
[2] Tavian L et. al., Towards the conceptual design of the cryogenic system of the Future Circular Collider, presented at the CEC 2017, Madison (WI), USA
[3] Kotnig C and Tavian L, Preliminary design of the beam screen cooling for the Future Circular Collider of hadron beams, IOP Conf. Series Vol **101** 012043
[4] Kotnig C, Tavian L and Brenn G, Investigation and performance assessment of hydraulic schemes for the beam screen cooling for the Future Circular Collider of hadron beams, IOP Conference Series **171** 012006
[5] Kloeppel S, Quack H, Haberstroh C and Holdener, Neon helium mixtures as a refrigerant for the FCC beam screen cooling: comparison of cycle design options, IOP Conf. Series Vol **101** 012042